Scientia Iranica B (2015) 22(2), 561–577

SCIENTIA IRANICA

Sharif University of Technology
Scientia Iranica
Transactions B: Mechanical Engineering
www.scientiairanica.com

Research Note

Thermo-elastic bending analysis of functionally graded sandwich plates by hyperbolic shear deformation theory

J. Rouzegar* **and M. Gholami**

Department of Aerospace and Mechanical Engineering, Shiraz University of Technology, Shiraz, P.O. Box 71555-313, Iran.

Received 24 November 2013; received in revised form 9 May 2014; accepted 9 August 2014

KEYWORDS
Extension effect;
FG material;
Hyperbolic plate theory;
Sandwich plate;
Thermo-elastic analysis.

Abstract. The thermo-elastic bending analysis of functionally graded ceramic-metal sandwich plates is presented in this study. The sandwich plate faces are assumed to be homogeneous and the core layer is constructed from FG material which its properties are varied through thickness according to the power-law equation. The hyperbolic shear deformation theory considering extension effect is employed for modeling the FG ceramic-metal sandwich plates. The presented theory is variationally consistent, does not require shear correction factor, and gives rise to transverse shear stress varying parabolically across the thickness. The governing equations are derived from principle of virtual work and the closed-form solutions are obtained using Navier method. The consideration of extension effect in presented formulation is examined and it is found that though it has no noticeable effect on transverse deflections and in-plane normal stresses, the obtained transverse shear stresses are quite affected by this term. Also the effects of thermal load, aspect ratio, thickness aspect ratio, thickness to side ratio and volume fraction index are investigated. It is observed that presented method is accurate and simple to use in comparison to other higher order shear deformation plate theories.

1. Introduction

Functionally Graded Materials (FGMs) were proposed by the Japanese researchers in 1984 [1,2]. They overcome the interface problems and discontinuity in stress distribution of the previous materials, such as combination of elastic laminates bounded together. These novel materials are microscopically inhomogeneous and characterized by a gradual change in material properties over volume. Due to their effective properties, functionally graded structures are widely utilized in many industries, such as high efficiency engine components, light weight structures for aircrafts and space industries, shipbuilding industries, medical instruments, biomechanics and automotive industries. One of the most important FGMs is metal-ceramic combination which gains superior properties than each constituent, in which ceramic phase protects metal phase from extreme heat environments, corrosion and oxidation. This property can be utilized in controlling thermal stresses in elements exposed to high temperatures, such as gas turbine blades and aerospace structures.

Many studies on analysis of FGMs behaviors have been performed in recent years [3,4]. Zenkour presented an analytical solution for bending of cross-ply laminates under thermo-mechanical loads [5]. Zenkour and Alghamdi studied thermo-elastic bending of sandwich plates with ceramic core and FG metal-ceramic faces using simplified refined sinusoidal shear deformation plate theory [6]. Various analyses of FGMs were investigated based on the meshless methods by several researchers [7-9]. Kashtalian investigated the

*. *Corresponding author. Tel./Fax: +98 711 7264102*
E-mail address: rouzegar@sutech.ac.ir (J. Rouzegar)

bending response of FG plates using the 3D elasticity solution [10]. Vel and Batra presented a 3D solution for vibration analysis of FGMs [11]. Reddy analyzed the FG composite laminates plates using the Equivalent Single Layer (ESL) and layerwise theories [12]. Lanhe studied the thermal buckling of simply supported moderately thick FGM plates by implementation of first order shear deformation theory [13]. Zhao et al. performed mechanical and thermal buckling analysis of FG plates using element-free kp-Ritz method [14]. Praveen and Reddy studied the nonlinear transient thermo-elastic response of functionally graded plates using finite element method [15]. Reddy and Chin gave a nice overview of thermo-mechanical behavior of functionally graded cylinders and plates [16].

The Classical Plate Theory (CPT) is the simplest plate theory that gives reasonable results for moderately thin plates but cannot predict the transverse shear stresses along the thickness [17]. The First-order Shear Deformation Theory (FSDT) predicts the constant transverse shear stress along the plate thickness [18,19]. In this theory, the shear correction factor is required and the free stress condition on the plate surfaces is not satisfied. To avoid the use of shear correction factor, the Higher-order Shear Deformation Theories (HSDTs) were developed [20-23].

Recently, some new HSDTs have been introduced. Shimpi presented a two-variable refined plate theory for isotropic and orthotropic plates which involves only two unknown functions [24,25]. Kim et al. studied the laminate composite plate behaviors using two-variable refined plate theory considering the extension effect [26]. El Meiche et al. presented a new hyperbolic shear deformation plate theory for buckling and vibration analyses of FGM sandwich plates [27]. Mantari and Soares developed a new trigonometric higher order plate theory with extension effect for analysis of functionally graded plates [28]. Tounsi et al. developed a refined trigonometric shear deformation theory for thermo-elastic bending of FGM sandwich plates [29]. Mantari et al. presented a new accurate higher order shear deformation theory for bending and free vibration analysis of isotropic and multilayered plates and shells [30]. Vidal and Polit developed a refined sinus plate finite element formulation and investigated the effects of mechanical and thermal loads on laminated and sandwich structures [31]. Zenkour and Sobhy studied the dynamic bending response of FG plates resting on elastic foundation using sinusoidal shear deformation plate theory [32]. Houari et al. presented a new higher order shear and normal deformation theory for thermo-elastic bending analysis of FG sandwich plates [33]. Wang and Shi introduced a simple and accurate sandwich plate theory accounting for transverse normal strain and interfacial stress continuity [34]. Mantari and Soares presented an optimized sinusoidal higher order shear deformation theory for bending analysis of FG plates and shells [35].

In this paper, an analytical solution for thermo-elastic bending of FG sandwich plates is presented using the hyperbolic shear deformation plate theory. The displacement field is assumed to vary hyperbolically across the plate thickness. The presented theory satisfies free stress boundary conditions at top and bottom surfaces of plate without using the shear correction factor. Also the consideration of extension effect is investigated in presented formulation and the obtained results are compared with some HSDTs with five unknown functions to illustrate simplicity, efficiency and accuracy of presented formulations. Some of these HSDTs which are utilized in this study are: Parabolic Shear Deformation Plate Theory (PSDPT) by Reddy [21], Sinusoidal Shear Deformation Plate Theory (SSDPT) by Tourtier [36], and Exponential Shear Deformation Plate Theory (ESDPT) by Karama et al. [37].

2. Problem formulation

In the present study, a rectangular FG Ceramic-Metal sandwich plate with uniform thickness composed of three different layers is studied. Top and bottom faces are constituted of isotropic ceramic and metal phases, respectively, and the core is made of FG material. The right-handed Cartesian coordinate system is used in which plate lies in x-y plane, z axis is normal to the plate along thickness and the mid-plane is located at $z = 0$, as illustrated in Figure 1.

Top plate coordinate is $z = z_3 = +h/2$ and the bottom is $z = z_0 = -h/2$. Also the two interfaces coordinates are z_1 and z_2 form bottom to top through the thickness, as shown in Figure 2.

Material properties of the FG core are assumed to vary through the thickness according to the power law. From the mixture law [38], the following relation can be written for effective material properties of the

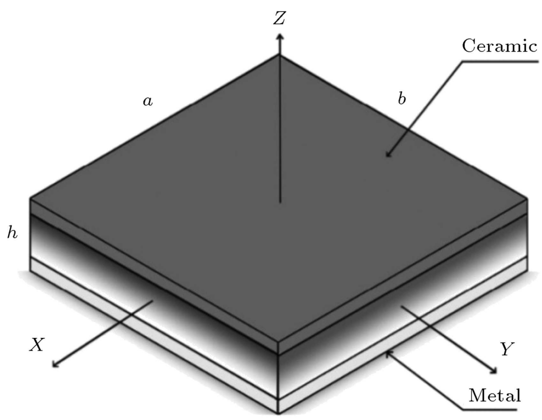

Figure 1. Geometry of rectangular FG sandwich plate in rectangular Cartesian coordinates.

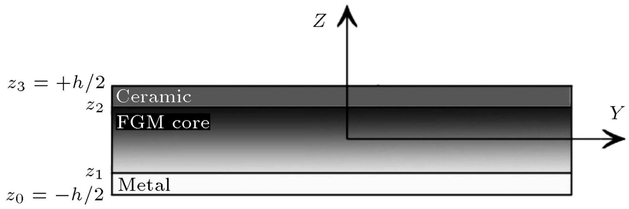

Figure 2. Variation of the plate constituents along the thickness of FG sandwich plate.

plate:

$$\begin{Bmatrix} P^{(3)}(z) \\ P^{(2)}(z) \\ P^{(1)}(z) \end{Bmatrix} = \begin{Bmatrix} P_3 & z_2 \le z \le z_3 \\ P_1 + (P_3 - P_1)\left(\frac{z-z_1}{z_2-z_1}\right)^k & z_1 \le z \le z_2 \\ P_1 & z_0 \le z \le z_1 \end{Bmatrix}. \tag{1}$$

Here, $P(z)$ can be Young's modulus, E, or thermal expansion, α. Indexes 1, 2 and 3 express the properties of layers 1, 2 and 3 form bottom to top of the plate, respectively. k is the volume fraction index ($0 \le k \le +\infty$), which indicates the variation of material properties of FG core through the thickness from metallic phase at the bottom interface to ceramic phase at the top interface. For sake of simplicity, Poisson's ratio is assumed to be constant due to Chi and Chung works [39] which this assumption is utilized in various literatures [21,29,36-37].

2.1. Higher-order displacement theory

Higher-order plate theories assume the following displacement field in Cartesian coordinates:

$$u = u_0(x, y) - z\frac{\partial w_0}{\partial x} + \psi(z)\theta_x, \tag{2a}$$

$$v = v_0(x, y) - z\frac{\partial w_0}{\partial y} + \psi(z)\theta_y, \tag{2b}$$

$$w = w_0(x, y), \tag{2c}$$

where u, v and w are the displacements in the x, y and z directions and u_0, v_0 and w_0 are the mid-plane displacements. θ_x is the rotation of the yz plane about the y axis and θ_y is the rotation of the xz plane about x axis. Main difference of the higher-order theories concern to definition of shape function $\psi(z)$. Several shape functions have been introduced by different researchers which some of them are as below:

Classical Plate Theory (CLPT) [17]: $\psi(z) = 0$;

First-order Shear Deformation Plate Theory (FSDPT) [40]: $\psi(z) = z$;

Parabolic Shear Deformation Plate Theory (PSDPT) [21]: $\psi(z) = (1 - (4z^2)/(3h^2))$;

Sinusoidal Shear Deformation Plate Theory (SSDPT) [36]: $\psi(z) = (h/\pi)\sin(\pi z/h)$;

Exponential Shear Deformation Plate Theory (ESDPT) [37]: $\psi(z) = ze^{-2(z/h)^2}$.

2.2. Hyperbolic shear deformation plate theory

This theory satisfies stress free conditions at the top and bottom planes of the plate without need of shear correction factor. The displacements are assumed to be small in comparison to plate dimensions; so their derivatives and therefore the strains are infinitesimal. Considering extension effect, the transverse displacement (w) is composed of three components:

$$w(x, y, z) = w_b(x, y) + w_s(x, y) + w_a(x, y), \tag{3}$$

where w_b, w_s and w_a are bending, shear and extension parts of the transverse displacement, respectively. The in-plane displacements, u and v, are assumed as follows:

$$u = u_0 + u_b + u_s, \qquad v = v_0 + v_b + v_s, \tag{4}$$

where u_b and v_b are bending components, and u_s and v_s are shear components defined as below:

$$u_b = -z\frac{\partial w_b}{\partial x}, \qquad v_b = -z\frac{\partial w_b}{\partial y}, \tag{5a}$$

$$u_s = -f(z)\frac{\partial w_s}{\partial x}, \qquad v_s = -f(z)\frac{\partial w_s}{\partial y}, \tag{5b}$$

where:

$$f(z) = \frac{(h/\pi)\sinh\left(\frac{\pi}{h}z\right) - z}{[\cosh(\pi/2) - 1]}. \tag{6}$$

The strains can be obtained using the displacement field defined in Eqs. (3) and (4):

$$\begin{aligned}
\varepsilon_x &= \varepsilon_x^0 + zk_x^b + f(z)k_x^s, \\
\varepsilon_y &= \varepsilon_y^0 + zk_y^b + f(z)k_y^s, \\
\gamma_{xy} &= \gamma_{xy}^0 + zk_{xy}^b + f(z)k_{xy}^s, \\
\gamma_{yz} &= g(z)\gamma_{yz}^s + \gamma_{yz}^a, \\
\gamma_{xz} &= g(z)\gamma_{xz}^s + \gamma_{xz}^a, \qquad \varepsilon_z = 0,
\end{aligned} \tag{7}$$

where:

$$\begin{aligned}
&\varepsilon_x^0 = \frac{\partial u_0}{\partial x}, \qquad \varepsilon_y^0 = \frac{\partial v_0}{\partial y}, \qquad \gamma_{xy}^0 = \frac{\partial u_0}{\partial y} + \frac{\partial v_0}{\partial x}, \\
&k_x^b = -\frac{\partial^2 w_b}{\partial x^2}, \qquad k_y^b = -\frac{\partial^2 w_b}{\partial y^2}, \qquad k_{xy}^b = -2\frac{\partial^2 w_b}{\partial x \partial y}, \\
&k_x^s = -\frac{\partial^2 w_s}{\partial x^2}, \qquad k_y^s = -\frac{\partial^2 w_s}{\partial y^2}, \qquad k_{xy}^s = -2\frac{\partial^2 w_s}{\partial x \partial y}, \\
&\gamma_{yz}^s = \frac{\partial w_s}{\partial y}, \qquad \gamma_{xz}^s = \frac{\partial w_s}{\partial x}, \qquad \gamma_{yz}^a = \frac{\partial w_a}{\partial y}, \\
&\gamma_{xz}^a = \frac{\partial w_a}{\partial x}, \qquad g(z) = 1 - \frac{df(z)}{dz}.
\end{aligned} \tag{8}$$

The normal stress σ_z is negligible in comparison to in-plane stresses, σ_x and σ_y, and may be neglected in constitutive equations. The stress components for isotropic FGMs can be obtained by the following thermo-elastic constitutive relations:

$$\begin{Bmatrix} \sigma_x \\ \sigma_y \\ \tau_{xy} \end{Bmatrix}^{(n)} = \begin{bmatrix} Q_{11} & Q_{12} & 0 \\ Q_{12} & Q_{22} & 0 \\ 0 & 0 & Q_{66} \end{bmatrix}^{(n)} \begin{Bmatrix} \varepsilon_x - \alpha(z)T \\ \varepsilon_y - \alpha(z)T \\ \gamma_{xy} \end{Bmatrix}^{(n)}, \tag{9a}$$

$$\begin{Bmatrix} \tau_{yz} \\ \tau_{xz} \end{Bmatrix}^{(n)} = \begin{bmatrix} Q_{44} & 0 \\ 0 & Q_{55} \end{bmatrix}^{(n)} \begin{Bmatrix} \gamma_{yz} \\ \gamma_{xz} \end{Bmatrix}^{(n)}, \tag{9b}$$

where n is the layer number. Coefficients of the stiffness matrix in Eqs. (9a) and (9b) can be expressed as:

$$Q_{11} = Q_{22} = \frac{E(z)}{1-\nu^2}, \tag{10a}$$

$$Q_{12} = \frac{\nu E(z)}{1-\nu^2}, \tag{10b}$$

$$Q_{44} = Q_{55} = Q_{66} = \frac{E(z)}{2(1+\nu)}. \tag{10c}$$

The Young's modulus, $E(z)$, and thermal expansion coefficient, $\alpha(z)$, for FG core depend on the z coordinate and they vary through the thickness according to Eq. (1).

2.3. Governing equations

Using the principle of virtual work, the governing equation of present FG sandwich plate can be derived:

$$\int_V (\sigma_x \delta\varepsilon_x + \sigma_y \delta\varepsilon_y + \tau_{xy}\delta\gamma_{xy} + \tau_{yz}\delta\gamma_{yz} + \tau_{xz}\delta\gamma_{xz}) dV = 0, \tag{11}$$

where V is volume of the plate. Eq. (11) can be written in terms of coefficients of stiffness matrix by substituting the stresses and strains and integrating through the plate thickness:

$$\begin{aligned} \int_A \{ & N_x \delta\varepsilon_x^0 + N_y \delta\varepsilon_y^0 + N_{xy}\delta\gamma_{xy}^0 + M_x^b \delta\kappa_x^b + M_y^b \delta\kappa_y^b \\ & + M_{xy}^b \delta\kappa_{xy}^b + M_x^s \delta\kappa_x^s + M_y^s \delta\kappa_y^s + M_{xy}^s \delta\kappa_{xy}^s \\ & + Q_{yz}^a \delta\gamma_{yz}^a + Q_{xz}^a \delta\gamma_{xz}^a + Q_{yz}^s \delta\gamma_{yz}^s \\ & + Q_{xz}^s \delta\gamma_{xz}^s \} dxdy = 0, \end{aligned} \tag{12}$$

where A is the mid-plane area, (M_x, M_y) are bending moments, M_{xy} is twisting moment, and (N_x, N_y) and (Q_{xz}, Q_{yz}) are normal and shear forces, respectively. These resultants can be derived by integrating the corresponding stresses through the thickness of the layers as:

$$\begin{aligned} (N_x, N_y, N_{xy}) &= \int_{-h/2}^{h/2} (\sigma_x, \sigma_y, \tau_{xy}) dz \\ &= \sum_{n=0}^{2} \int_{z_n}^{z_{n+1}} (\sigma_x, \sigma_y, \tau_{xy}) dz, \\ (M_x^b, M_y^b, M_{xy}^b) &= \int_{-h/2}^{h/2} (\sigma_x, \sigma_y, \tau_{xy}) z dz \\ &= \sum_{n=0}^{2} \int_{z_n}^{z_{n+1}} (\sigma_x, \sigma_y, \tau_{xy}) z dz, \\ (M_x^s, M_y^s, M_{xy}^s) &= \int_{-h/2}^{h/2} (\sigma_x, \sigma_y, \tau_{xy}) f(z) dz \\ &= \sum_{n=0}^{2} \int_{z_n}^{z_{n+1}} (\sigma_x, \sigma_y, \tau_{xy}) f(z) dz, \\ (Q_{xz}^a, Q_{yz}^a, Q_{xz}^s, Q_{yz}^s) &= \int_{-h/2}^{h/2} (\tau_{xz}, \tau_{yz}, g(z)\tau_{xz}, g(z)\tau_{yz}) dz \\ &= \sum_{n=0}^{2} \int_{z_n}^{z_{n+1}} (\tau_{xz}, \tau_{yz}, g(z)\tau_{xz}, g(z)\tau_{yz}) dz. \end{aligned} \tag{13}$$

Substituting Eq. (7) in Eq. (9), integrating through the plate thickness, and using the definitions of stress resultants from Eq. (13), the following equations will be obtained:

$$\begin{Bmatrix} N \\ M^b \\ M^s \end{Bmatrix} = \begin{bmatrix} A & B & B^s \\ B & D & D^s \\ B^s & D^s & H^s \end{bmatrix} \begin{Bmatrix} \varepsilon \\ \kappa^b \\ \kappa^s \end{Bmatrix} - \begin{Bmatrix} N^T \\ M^{bT} \\ M^{sT} \end{Bmatrix}, \tag{14a}$$

$$\begin{Bmatrix} Q^a \\ Q^s \end{Bmatrix} = \begin{bmatrix} A^s & A^a \\ A^a & A^{ss} \end{bmatrix} \begin{Bmatrix} \gamma^a \\ \gamma^s \end{Bmatrix}, \tag{14b}$$

where:

$$N = \{N_x, N_y, N_{xy}\}^t, \qquad M^b = \{M_x^b, M_y^b, M_{xy}^b\}^t,$$

$$M^s = \{M_x^s, M_y^s, M_{xy}^s\}^t, \qquad N^T = \{N_x^T, N_y^T, 0\}^t,$$

$$M^{bT} = \{M_x^{bT}, M_y^{bT}, 0\}^t, \qquad M^{sT} = \{M_x^{sT}, M_y^{sT}, 0\}^t,$$

$$\varepsilon = \{\varepsilon_x^0, \varepsilon_y^0, \gamma_{xy}^0\}^t,$$

$$\kappa^b = \{\kappa_x^b, \kappa_y^b, \kappa_{xy}^b\}^t, \qquad \kappa^s = \{\kappa_x^s, \kappa_y^s, \kappa_{xy}^s\}^t,$$

$$Q^a = \{Q_{yz}^a, Q_{xz}^a\}^t, \qquad Q^s = \{Q_{yz}^s, Q_{xz}^s\}^t,$$

$$\gamma^a = \{\gamma_{yz}^a, \gamma_{xz}^a\}^t, \qquad \gamma^s = \{\gamma_{yz}^s, \gamma_{xz}^s\}^t, \tag{15a}$$

$$A = \begin{bmatrix} A_{11} & A_{12} & 0 \\ A_{12} & A_{22} & 0 \\ 0 & 0 & A_{66} \end{bmatrix},$$

$$B = \begin{bmatrix} B_{11} & B_{12} & 0 \\ B_{12} & B_{22} & 0 \\ 0 & 0 & B_{66} \end{bmatrix},$$

$$D = \begin{bmatrix} D_{11} & D_{12} & 0 \\ D_{12} & D_{22} & 0 \\ 0 & 0 & D_{66} \end{bmatrix},$$

$$B^s = \begin{bmatrix} B_{11}^s & B_{12}^s & 0 \\ B_{12}^s & B_{22}^s & 0 \\ 0 & 0 & B_{66}^s \end{bmatrix},$$

$$D^s = \begin{bmatrix} D_{11}^s & D_{12}^s & 0 \\ D_{12}^s & D_{22}^s & 0 \\ 0 & 0 & D_{66}^s \end{bmatrix},$$

$$H^s = \begin{bmatrix} H_{11}^s & H_{12}^s & 0 \\ H_{12}^s & H_{22}^s & 0 \\ 0 & 0 & H_{66}^s \end{bmatrix},$$

$$A^s = \begin{bmatrix} A_{44}^s & 0 \\ 0 & A_{55}^s \end{bmatrix}, \qquad A^{ss} = \begin{bmatrix} A_{44}^{ss} & 0 \\ 0 & A_{55}^{ss} \end{bmatrix},$$

$$A^a = \begin{bmatrix} A_{44}^a & 0 \\ 0 & A_{55}^a \end{bmatrix}, \tag{15b}$$

where A_{ij}, B_{ij} etc. are coefficients of the plate stiffness, defined by:

$$(A_{ii}, B_{ii}, D_{ii}, B_{ii}^s, D_{ii}^s, H_{ii}^s) = \sum_{n=0}^{2} \int_{z_n}^{z_{n+1}} Q_{ii}^{(n)} [1, z, z^2, f(z), zf(z), f^2(z)] dz,$$

$$(i = 1, 2), \tag{16a}$$

$$(A_{12}, B_{12}, D_{12}, B_{12}^s, D_{12}^s, H_{12}^s) = \sum_{n=0}^{2} \int_{z_n}^{z_{n+1}} Q_{12}^{(n)} [1, z, z^2, f(z), zf(z), f^2(z)] dz, \tag{16b}$$

$$(A_{66}, B_{66}, D_{66}, B_{66}^s, D_{66}^s, H_{66}^s) = \sum_{n=0}^{2} \int_{z_n}^{z_{n+1}} Q_{66}^{(n)} [1, z, z^2, f(z), zf(z), f^2(z)] dz, \tag{16c}$$

$$A_{ii}^s = \sum_{n=0}^{2} \int_{z_n}^{z_{n+1}} Q_{ii}^{(n)} dz, \qquad (i = 4, 5), \tag{16d}$$

$$A_{ii}^{ss} = \sum_{n=0}^{2} \int_{z_n}^{z_{n+1}} Q_{ii}^{(n)} [g(z)]^2 dz, \qquad (i = 4, 5), \tag{16e}$$

$$A_{ii}^a = \sum_{n=0}^{2} \int_{z_n}^{z_{n+1}} Q_{ii}^{(n)} [g(z)] dz, \qquad (i = 4, 5). \tag{16f}$$

Also, N^T and (M^{bT}, M^{sT}) are thermal force and moment resultants, respectively. In the present study, the material properties are constant in x and y directions and therefore we can write:

$$N_x^T = N_y^T, \qquad M_x^{bT} = M_y^{bT}, \qquad M_x^{sT} = M_y^{sT}. \tag{17}$$

Thermal resultants can be written in terms of material properties of plate as:

$$\begin{Bmatrix} N_x^T \\ M_x^{bT} \\ M_x^{sT} \end{Bmatrix} = \sum_{n=0}^{2} \int_{z_n}^{z_{n+1}} \frac{E(z)}{1-\nu} \alpha(z) T \begin{Bmatrix} 1 \\ z \\ f(z) \end{Bmatrix} dz. \tag{18}$$

The temperature field is assumed to be a combination of three terms according to Eq. (19). The first term regards uniform temperature field across the thickness, the second term considers the contribution of temperature which linearly varies across the thickness and the last term considers the temperature variation through the thickness according to the shape function of the theory. This temperature field was utilized in several previous works [6,29,30] and results of present study will be compared with existing ones in literature.

$$T(x, y, z) = T_1(x, y) + \frac{z}{h} T_2(x, y) + \frac{\psi(z)}{h} T_3(x, y). \tag{19}$$

Substituting Eqs. (7) and (8) into Eq. (12), integrating by parts and setting the coefficients of δu_0, δv_0, δw_b, δw_s and δw_a to zero separately, the following governing equations will be obtained:

$$\delta u_0 : \quad \frac{\partial N_x}{\partial x} + \frac{\partial N_{xy}}{\partial y} = 0, \tag{20a}$$

$$\delta v_0 : \quad \frac{\partial N_{xy}}{\partial x} + \frac{\partial N_y}{\partial y} = 0, \tag{20b}$$

$$\delta w_b : \quad \frac{\partial^2 M_x^b}{\partial x^2} + 2\frac{\partial^2 M_{xy}^b}{\partial x \partial y} + \frac{\partial^2 M_y^b}{\partial y^2} = 0, \tag{20c}$$

$$\delta w_s: \quad \frac{\partial^2 M_x^s}{\partial x^2}+2\frac{\partial^2 M_{xy}^s}{\partial x\partial y}+\frac{\partial^2 M_y^s}{\partial y^2}+\frac{\partial Q_{xz}^s}{\partial x}+\frac{\partial Q_{yz}^s}{\partial y}=0, \tag{20d}$$

$$\delta w_a: \quad \frac{\partial Q_{xz}^a}{\partial x}+\frac{\partial Q_{yz}^a}{\partial y}=0. \tag{20e}$$

Substituting Eqs. (14), (7) and (8) into Eqs. (20), the governing equations in terms of displacements will be obtained:

$$A_{11}\frac{\partial^2 u_0}{\partial x^2}+A_{66}\frac{\partial^2 u_0}{\partial y^2}+(A_{12}+A_{66})\frac{\partial^2 v_0}{\partial x\partial y}-\left[B_{11}\frac{\partial^3 w_b}{\partial x^3}+(B_{12}+2B_{66})\frac{\partial^3 w_b}{\partial x\partial y^2}\right]-\left[B_{11}^s\frac{\partial^3 w_s}{\partial x^3}+(B_{12}^s+2B_{66}^s)\frac{\partial^3 w_s}{\partial x\partial y^2}\right]=F_1, \tag{21a}$$

$$(A_{12}+A_{66})\frac{\partial^2 u_0}{\partial x\partial y}+A_{66}\frac{\partial^2 v_0}{\partial x^2}+A_{22}\frac{\partial^2 v_0}{\partial y^2}-\left[(B_{12}+2B_{66})\frac{\partial^3 w_b}{\partial x^2\partial y}+B_{22}\frac{\partial^3 w_b}{\partial y^3}\right]-\left[(B_{12}^s+2B_{66}^s)\frac{\partial^3 w_s}{\partial x^2\partial y}+B_{22}^s\frac{\partial^3 w_s}{\partial y^3}\right]=F_2, \tag{21b}$$

$$B_{11}\frac{\partial^3 u_0}{\partial x^3}+(B_{12}+2B_{66})\frac{\partial^3 u_0}{\partial x\partial y^2}+(B_{12}+2B_{66})\frac{\partial^3 v_0}{\partial x^2\partial y}+B_{22}\frac{\partial^3 v_0}{\partial y^3}-\left[D_{11}\frac{\partial^4 w_b}{\partial x^4}+2(D_{12}+2D_{66})\frac{\partial^4 w_b}{\partial x^2\partial y^2}+D_{22}\frac{\partial^4 w_b}{\partial y^4}\right]-\left[D_{11}^s\frac{\partial^4 w_s}{\partial x^4}+2(D_{12}^s+2D_{66}^s)\frac{\partial^4 w_s}{\partial x^2\partial y^2}+D_{22}^s\frac{\partial^4 w_s}{\partial y^4}\right]=F_3, \tag{21c}$$

$$B_{11}^s\frac{\partial^3 u_0}{\partial x^3}+(B_{12}^s+2B_{66}^s)\frac{\partial^2 u_0}{\partial x\partial y^2}+(B_{12}^s+2B_{66}^s)\frac{\partial^3 v_0}{\partial x^2\partial y}+B_{22}^s\frac{\partial^3 v_0}{\partial y^3}-\left[D_{11}^s\frac{\partial^4 w_b}{\partial x^4}+2(D_{12}^s+2D_{66}^s)\frac{\partial^4 w_b}{\partial x^2\partial y^2}+D_{22}^s\frac{\partial^4 w_b}{\partial y^4}\right]-\left[H_{11}^s\frac{\partial^4 w_s}{\partial x^4}+2(H_{12}^s+2H_{66}^s)\frac{\partial^4 w_s}{\partial x^2\partial y^2}+H_{22}^s\frac{\partial^4 w_s}{\partial y^4}\right]+A_{55}^a\frac{\partial^2 w_a}{\partial x^2}+A_{44}^a\frac{\partial^2 w_a}{\partial y^2}+A_{55}^s\frac{\partial^2 w_s}{\partial x^2}+A_{44}^s\frac{\partial^2 w_s}{\partial y^2}=F_4, \tag{21d}$$

$$A_{55}\frac{\partial^2 w_a}{\partial x^2}+A_{44}\frac{\partial^2 w_a}{\partial y^2}+A_{55}^a\frac{\partial^2 w_s}{\partial x^2}+A_{44}^a\frac{\partial^2 w_s}{\partial y^2}=F_5, \tag{21e}$$

where F_1, F_2, F_3, F_4 and F_5 are the thermal resultants force, defined by:

$$F_1=\frac{\partial N_x^T}{\partial x}, \qquad F_2=\frac{\partial N_y^T}{\partial y},$$

$$F_3=\frac{\partial^2 M_x^{bT}}{\partial x^2}+\frac{\partial^2 M_y^{bT}}{\partial y^2},$$

$$F_4=\frac{\partial^2 M_x^{sT}}{\partial x^2}+\frac{\partial^2 M_y^{sT}}{\partial y^2},$$

$$F_5=0. \tag{22}$$

3. Analytical solution procedure

The boundary of FG sandwich plate is assumed to be simply supported at all edges which leads to the boundary conditions:

$$v_0=w_b=w_s=w_a=N_x=M_x^b=M_x^s=0$$

$$\text{at} \quad x=0,a,$$

$$u_0=w_b=w_s=w_a=N_y=M_y^b=M_y^s=0$$

$$\text{at} \quad y=0,b. \tag{23}$$

The Navier method is employed for solution of obtained governing equations. The displacements fields are sought as the following expressions which satisfy the above boundary conditions automatically:

$$\begin{Bmatrix} u_0 \\ v_0 \\ w_b \\ w_s \\ w_a \end{Bmatrix}=\sum_{m=1}^{\infty}\sum_{n=1}^{\infty}\begin{Bmatrix} U_{mn}\cos(\lambda x)\sin(\mu y) \\ V_{mn}\sin(\lambda x)\cos(\mu y) \\ W_{bmn}\sin(\lambda x)\sin(\mu y) \\ W_{smn}\sin(\lambda x)\sin(\mu y) \\ W_{amn}\sin(\lambda x)\sin(\mu y) \end{Bmatrix}, \tag{24}$$

where U_{mn}, V_{mn}, W_{bmn}, W_{smn} and W_{amn} are unknown coefficients to be determined in the solution procedure.

In this study, the temperature distribution in x-y plane are assumed to be uniform and sinusoidal. For sinusoidal distribution temperature field we have:

$$\{T\}=\{\overline{T}\}\sin(\lambda x)\sin(\mu y),$$

$$T=\{T_1,T_2,T_3\}^t, \qquad \overline{T}=\{\overline{T}_1,\overline{T}_2,\overline{T}_3\}^t, \tag{25}$$

where T_1, T_2 and T_3 were defined in Eq. (19). The double Fourier expansion of uniformly distributed temperature can be expressed as follows:

$$\{T\} = \{\overline{T}\} \sum_{m=1}^{\infty} \sum_{n=1}^{\infty} \frac{16}{mn\pi^2} \sin(\lambda x) \sin(\mu y)$$

$$m, n = 1, 3, 5 \cdots \tag{26}$$

in which $\lambda = m\pi/a$ and $\mu = n\pi/b$.

Substituting Eqs. (24)-(26) in governing Eqs. (21), the following system of equations is obtained:

$$[K]\{\Delta\} = \{F\}, \tag{27}$$

where:

$$\{\Delta\} = \left\{U_{mn}, V_{mn}, W^b_{mn}, W^s_{mn}, W^a_{mn}\right\}^t,$$

is displacement vector which should be determined, $[K]$ is the stiffness matrix, and $\{F\}$ is the force vector. Components of symmetric $[K]$ matrix are as follows:

$$[K] = \begin{bmatrix} a_{11} & a_{12} & a_{13} & a_{14} & a_{15} \\ a_{21} & a_{22} & a_{23} & a_{24} & a_{25} \\ a_{31} & a_{32} & a_{33} & a_{34} & a_{35} \\ a_{41} & a_{42} & a_{43} & a_{44} & a_{45} \\ a_{51} & a_{52} & a_{53} & a_{54} & a_{55} \end{bmatrix}, \tag{28}$$

where:

$$a_{11} = -(A_{11}\lambda^2 + A_{66}\mu^2),$$

$$a_{12} = -\lambda\mu(A_{12} + A_{66}),$$

$$a_{13} = -\lambda[B_{11}\lambda^2 + (B_{12} + 2B_{66})\mu^2],$$

$$a_{14} = -\lambda[B^s_{11}\lambda^2 + (B^s_{12} + 2B^s_{66})\mu^2],$$

$$a_{22} = -(A_{66}\lambda^2 + A_{22}\mu^2),$$

$$a_{23} = \mu[(B_{12} + 2B_{66})\lambda^2 + B_{22}\mu^2],$$

$$a_{24} = \mu[(B^s_{12} + 2B^s_{66})\lambda^2 + B^s_{22}\mu^2],$$

$$a_{33} = -(D_{11}\lambda^4 + 2(D_{12} + 2D_{66})\lambda^2\mu^2 + D_{22}\mu^4),$$

$$a_{34} = -(D^s_{11}\lambda^4 + 2(D^s_{12} + 2D^s_{66})\lambda^2\mu^2 + D^s_{22}\mu^4),$$

$$a_{44} = -\left(H^s_{11}\lambda^4 + 2(H^s_{11} + 2H^s_{66})\lambda^2\mu^2 + H^s_{22}\mu^4 + A^s_{55}\lambda^2 + A^s_{44}\mu^2 + A^s_{55}\lambda^2 + A^s_{44}\mu^2\right),$$

$$a_{45} = -(A^a_{55}\lambda^2 + A^a_{44}\mu^2),$$

$$a_{55} = -(A_{55}\lambda^2 + A_{44}\mu^2),$$

$$a_{15} = 0, \qquad a_{25} = 0, \qquad a_{35} = 0. \tag{29}$$

Furthermore, the force vector is composed of the following components:

$$\{F\} = \{F_1, F_2, F_3, F_4, F_5\}^t, \tag{30}$$

where:

$$F_1 = \lambda(A^T\overline{T}_1 + B^T\overline{T}_2 + B^{aT}\overline{T}_3),$$

$$F_2 = \mu(A^T\overline{T}_1 + B^T\overline{T}_2 + B^{aT}\overline{T}_3),$$

$$F_3 = -h(\lambda^2 + \mu^2)(B^T\overline{T}_1 + D^T\overline{T}_2 + D^{aT}\overline{T}_3),$$

$$F_4 = -h(\lambda^2 + \mu^2)(B^{sT}\overline{T}_1 + D^{sT}\overline{T}_2 + F^{sT}\overline{T}_3),$$

$$F_5 = 0, \tag{31}$$

and:

$$\{A^T, B^T, D^T\} = \sum_{n=0}^{2} \int_{z_n}^{z_{n+1}} \frac{E(z)}{1-\nu^2}(1+\nu)\alpha(z)\left\{1, \overline{z}, \overline{z}^2\right\} dz,$$

$$\{B^{aT}, D^{aT}\} = \sum_{n=0}^{2} \int_{z_n}^{z_{n+1}} \frac{E(z)}{1-\nu^2}(1+\nu)\alpha(z)\overline{\psi}(z)\left\{1, \overline{z}\right\} dz,$$

$$\{B^{sT}, D^{sT}, F^{sT}\} = \sum_{n=0}^{2} \int_{z_n}^{z_{n+1}} \frac{E(z)}{1-\nu^2}(1+\nu)\alpha(z)\overline{f}(z)\left\{1, \overline{z}, \overline{\psi}(z)\right\} dz. \tag{32}$$

Also, we have:

$$\overline{z} = z/h, \quad \overline{f}(z) = f(z)/h, \quad \overline{\psi}(z) = \psi(z)/h. \tag{33}$$

4. Numerical results and discussion

In this section employing hyperbolic shear deformation plate theory and considering extension effect, several numerical examples of simply supported FG sandwich plate under thermo-mechanical loading are solved. In order to validate the presented method, obtained results are compared with first and higher order plate theories. The materials used in this study are Titanium and Zirconia whose properties are shown in Table 1. The Poisson's ratios for both ceramic and metallic phases are assumed to be constant and independent of temperature.

The temperature distribution across plate thickness is considered according to Eq. (19); it means that as well as investigation on linear distribution of

Table 1. Material properties of FG sandwich plate.

Properties	Metal: Ti-6A-4V	Ceramic: ZrO_2
$E(\mathrm{GP}_a)$	66.2	117.0
v	1/3	1/3
$\alpha(10^{-6}/\mathrm{K})$	10.3	7.11

temperature across the thickness, the effects of thermal load values $\overline{T}_1$ and $\overline{T}_3$ are also studied. As mentioned before, the temperature distribution in x and y directions are uniform and sinusoidal whose Fourier expansions were described by Eqs. (25) and (26). For sake of brevity and to express the thickness ratio of each layer, a combination of three numbers (called "thickness aspect ratio") is employed; for example "1-2-1" defines the ratios of each layer from bottom to top, i.e. the thickness of FG core is twice the thickness of Metal and ceramic layers. The obtained results are presented in two cases: PERESENT 1 (the extension effect is not considered in formulation) and PERESENT 2 (the extension effect is considered in formulation). Dimensionless values used for transverse deflection, in-plane normal stress and transverse shear stresses are listed in Table 2, where $E_0 = 1$ GPa and $\alpha_0 = 10e-6/K$. It is assumed that $a/h = 10$, $a/b = 1$, $\overline{T}_1 = \overline{T}_3 = 0$ and $\overline{T}_2 = 0$, unless mentioned otherwise. The shear correction factor for FSDPT theory is $k = 5/6$.

Example 1. A simply supported rectangular FG sandwich plate subjected to temperature field varying linearly through the thickness and sinusoidally in x and y directions is considered.

In Table 3 the effects of volume fraction index (k) and thickness aspect ratio on dimensionless central deflection of square plate are investigated. It is observed that results of presented method are in good agreement with other theories. Results of PRESENT 1 and PRESENT 2 formulations are very close and it means that the extension term has no noticeable effect on the transverse deflections. For a constant thickness aspect ratio, increasing the volume fraction index significantly increases the deflection of the plate, since the behavior of FG core tends to metal phase and consequently the plate stiffness is decreased.

Table 4 contains the dimensionless central deflection of the plate for different aspect ratios and thickness aspect ratios. As expected, the transverse deflection is decreased when aspect ratio is increased in the result of plate stiffness increase. Also it is observed that results of the present formulations are very close and they are almost identical to other theories.

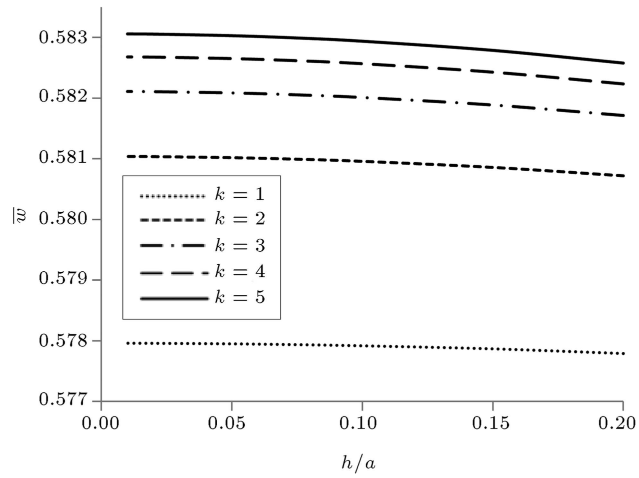

Figure 3. Effect of thickness to side ratio on the dimensionless transverse deflection, $\overline{w}$, for 1-2-1 FG sandwich plate.

Table 5 contains the effect of aspect ratio on the dimensionless transverse deflection considering different volume fraction indexes. For a constant volume fraction index the transverse deflection is decreased by increasing the aspect ratio, and for a specific aspect ratio the transverse deflection is increased by increasing the volume fraction index. The reasons of these issues were discussed before.

Figure 3 illustrates the effects of thickness to side ratio on the dimensionless transverse deflections considering different volume fraction indexes. As expected, for a certain volume fraction index, the deflections are decreased as the thickness to side ratio is increased and for a specific thickness to side ratio the deflections are increased as volume fraction index is increased.

The dimensionless in-plane normal stresses, $\overline{\sigma}_x$, have been tabulated in Table 6 for square plates ($a/b = 1$) considering different thickness aspect ratios and volume fraction indexes. The present formulations are in good agreement with other theories and again extension term has negligible effects on the result. It is observed that by increasing volume fraction ratio, the normal stresses, $\overline{\sigma}_x$, are decreased for 1-2-1 and 2-2-1

Table 2. Dimensionless parameters.

Dimensionless transverse deflection	$\overline{w} = \frac{h}{\alpha_0 \overline{T}_2 a^2} w\left(\frac{a}{2}, \frac{b}{2}, z\right)$
Dimensionless in-plane normal stress	$\overline{\sigma}_x = \frac{10h}{\alpha_0 \overline{T}_2 E_0 a^2} \sigma_x\left(\frac{a}{2}, \frac{b}{2}, \frac{h}{2}\right)$
Dimensionless transverse shear stress	$\overline{\tau}_{xz} = \frac{10h}{\alpha_0 \overline{T}_2 E_0 a} \tau_{xz}\left(0, \frac{b}{2}, 0\right)$

Table 3. Effects of volume fraction index and thickness aspect ratio on dimensionless central deflections $\overline{w}$ $(a/b = 1)$.

k	Theory	$\overline{w}$				
		1-1-1	1-2-1	1-2-2	2-1-2	2-2-1
$k=0$	PRESENT 1	0.5697923674	0.5560289302	0.5446015603	0.5762419990	0.5762419988
	PRESENT 2	0.5697906561	0.5560249740	0.5445992909	0.5762429690	0.5762429691
	PSDPT	0.5697963998	0.5560435002	0.5446190228	0.5762401048	0.5762401048
	SSDPT	0.5698014747	0.5560597437	0.5446403969	0.5762378652	0.5762378652
	ESDPT	0.5698069150	0.5560764877	0.5446621105	0.5762357284	0.5762357284
	FSDPT	0.5697678537	0.5559251873	0.5444491654	0.5762632835	0.5762632835
$k=1$	PRESENT 1	0.5788143493	0.5779191830	0.5730531291	0.5795149450	0.5826038457
	PRESENT 2	0.5788125914	0.5779173382	0.5730531161	0.5795131466	0.5825943606
	PSDPT	0.5788094857	0.5779144556	0.5730538443	0.5795096754	0.5825925248
	SSDPT	0.5788035048	0.5779086454	0.5730547792	0.5795031868	0.5825784716
	ESDPT	0.5787973877	0.5779027122	0.5730558373	0.5794965358	0.5825639272
	FSDPT	0.5788564684	0.5779602984	0.5730516734	0.5795600773	0.5826950408
$k=2$	PRESENT 1	0.5800516210	0.5809657676	0.5775582952	0.5800309116	0.5846167843
	PRESENT 2	0.5800467343	0.5809582911	0.5775576563	0.5800273615	0.5845986656
	PSDPT	0.5800449336	0.5809565819	0.5775550792	0.5800249852	0.5846012120
	SSDPT	0.5800366258	0.5809451600	0.5775511540	0.5800176471	0.5845817996
	ESDPT	0.5800280039	0.5809332994	0.5775471901	0.5800100670	0.5845616254
	FSDPT	0.5801060851	0.5810391437	0.5775881317	0.5800803280	0.5847396905
$k=3$	PRESENT 1	0.5804283619	0.5820222850	0.5789868553	0.5801944236	0.5858475020
	PRESENT 2	0.5804215261	0.5820105072	0.5789850412	0.5801899232	0.5858241087
	PSDPT	0.5804209150	0.5820109286	0.5789821524	0.5801882554	0.5858293185
	SSDPT	0.5804116250	0.5819967453	0.5789763660	0.5801805990	0.5858066376
	ESDPT	0.5804019295	0.5819819368	0.5789704450	0.5801726650	0.5857830725
	FSDPT	0.5804877232	0.5821107784	0.5790277184	0.5802453381	0.5859905852
$k=4$	PRESENT 1	0.5805920959	0.5825824613	0.5795840278	0.5802628946	0.5867252924
	PRESENT 2	0.5805840008	0.5825676430	0.5795812478	0.5802578147	0.5866985682
	PSDPT	0.5805842215	0.5825697358	0.5795786331	0.5802566082	0.5867053410
	SSDPT	0.5805743751	0.5825538083	0.5795719709	0.5802487952	0.5866804640
	ESDPT	0.5805640686	0.5825371384	0.5795651154	0.5802406844	0.5866546493
	FSDPT	0.5806541647	0.5826804850	0.5796297723	0.5803145105	0.5868825281
$k=5$	PRESENT 1	0.5806815193	0.5829554515	0.5798777615	0.5802966458	0.5873938994
	PRESENT 2	0.5806725539	0.5829384293	0.5798742542	0.5802911799	0.5873649698
	PSDPT	0.5806733607	0.5829417477	0.5798719991	0.5802902921	0.5873726768
	SSDPT	0.5806631440	0.5829245759	0.5798648672	0.5802823879	0.5873462331
	ESDPT	0.5806524307	0.5829065842	0.5798575047	0.5802741733	0.5873188309
	FSDPT	0.5807453814	0.5830603704	0.5799259999	0.5803486566	0.5875616248

and increased for 2-1-2. There is no regular change in stress values for 1-1-1 and 1-2-2 combinations.

The dimensionless in-plane normal stresses, $\overline{\sigma}_x$, through the plate thickness for ceramic, metal and FG sandwich plates are plotted in Figure 4 for different thickness aspect ratios. The in-plane normal stresses are negative for upper plane, positive for lower plane and zero at mid-plane for homogeneous ceramic and metal plates. For FG sandwich plates, no symmetry is observed for different thickness aspect ratios and the stresses are zero somewhere else than mid-plane. The continuity of stresses through the plate thickness is observed for all thickness aspect ratios.

Table 7 compares the dimensionless transverse

Table 4. Effect of thickness aspect ratio and aspect ratio (a/b) on dimensionless central deflections, $\overline{w}$ ($k=3$).

Thickness aspect ratio	Theory	$\bar{w}$				
		$a/b=1$	$a/b=2$	$a/b=3$	$a/b=4$	$a/b=5$
1-1-1	PRESENT 1	0.5804283619	0.2321357834	0.1160383311	0.0682335886	0.0445939819
	PRESENT 2	0.5804215261	0.2321292896	0.1160323970	0.0682284171	0.0445897564
	PSDPT	0.5804209150	0.2321283564	0.1160309371	0.0682262404	0.0445866922
	SSDPT	0.5804116250	0.2321190971	0.1160217287	0.0682171026	0.0445776442
	ESDPT	0.5804019295	0.2321094409	0.1160121379	0.0682076025	0.0445682591
	FSDPT	0.5804877232	0.2321950892	0.1160975447	0.0682926733	0.0446529018
1-2-1	PRESENT 1	0.5820222850	0.2327559023	0.1163338865	0.0683955472	0.0446899283
	PRESENT 2	0.5820105072	0.2327446399	0.1163234683	0.0683862793	0.0446820876
	PSDPT	0.5820109286	0.2327445763	0.1163226109	0.0683843417	0.0446788120
	SSDPT	0.5819967453	0.2327304399	0.1163085524	0.0683703912	0.0446649990
	ESDPT	0.5819819368	0.2327156920	0.1162939046	0.0683558823	0.0446506661
	FSDPT	0.5821107784	0.2328443114	0.1164221557	0.0684836210	0.0447777522
1-2-2	PRESENT 1	0.5789868553	0.2315702601	0.1157647758	0.0680802232	0.0445000151
	PRESENT 2	0.5789850412	0.2315686581	0.1157635213	0.0680794424	0.0444998225
	PSDPT	0.5789821524	0.2315655691	0.1157601052	0.0680755807	0.0444954087
	SSDPT	0.5789763660	0.2315598012	0.1157543682	0.0680698867	0.0444897690
	ESDPT	0.5789704450	0.2315539037	0.1157485096	0.0680640820	0.0444840329
	FSDPT	0.5790277184	0.2316110871	0.1158055437	0.0681209080	0.0445405937
2-1-2	PRESENT 1	0.5801944236	0.2320472672	0.1159982770	0.0682134745	0.0445837117
	PRESENT 2	0.5801899232	0.2320430494	0.1159945221	0.0682103506	0.0445813707
	PSDPT	0.5801882554	0.2320411153	0.1159921519	0.0682073873	0.0445776726
	SSDPT	0.5801805990	0.2320334841	0.1159845625	0.0681998556	0.0445702144
	ESDPT	0.5801726650	0.2320255820	0.1159767136	0.0681920803	0.0445625327
	FSDPT	0.5802453381	0.2320981354	0.1160490676	0.0682641573	0.0446342567
2-2-1	PRESENT 1	0.5858475020	0.2342532918	0.1170554092	0.0687976881	0.0449342363
	PRESENT 2	0.5858241087	0.2342307480	0.1170342640	0.0687784446	0.0449173527
	PSDPT	0.5858293185	0.2342351590	0.1170373604	0.0687797559	0.0449164528
	SSDPT	0.5858066376	0.2342125563	0.1170148873	0.0687574626	0.0448943883
	ESDPT	0.5857830725	0.2341890915	0.1169915887	0.0687343943	0.0448716118
	FSDPT	0.5859905852	0.2343962340	0.1171981170	0.0689400688	0.0450761989

shear stress, $\overline{\tau}_{xz}$, of the square FG sandwich plate considering different thickness aspect ratios and volume fraction ratios. Both the second and third terms of Eq. (19) are considered in temperature field distribution across the plate thickness. The shape function used in the refined plate theories determines the amount of shear deformation effects, and since different shape functions are used in higher order plate theories, the obtained transverse shear stresses listed in Table 7 are not identical. It is seen that the relative differences between the results for all thickness aspect ratios and volume fraction ratios are almost constant. Furthermore, applying extension effect in formulation leads to higher transverse shear stresses.

Figure 5 plots the distribution of dimensionless transverse shear stress, $\overline{\tau}_{xz}$, through the plate thickness for homogenous ceramic and metal plates and two FG sandwich plates ($k=1$ and $k=3$). It is assumed that $\overline{T}_3=-100$ and different thickness aspect ratios are examined. For ceramic and metal plates, symmetric distribution of transverse shear stresses is observed and maximum transverse shear stresses, $\overline{\tau}_{xz}$, are occurred at mid-plane of the plate; but for FG sandwich plates, no symmetry is observed and maxi-

Table 5. Effect of aspect ratio and volume fraction index on dimensionless central deflections, $\overline{w}$ (thickness aspect ratio: 1-2-1).

a/b	Theory	$\overline{w}$						
		Ceramic	$k=1$	$k=2$	$k=3$	$k=4$	$k=5$	**Metal**
1	PRESENT 1	0.5560289302	0.5779191830	0.5809657676	0.5820222850	0.5825824613	0.5829554515	0.5859292289
	PRESENT 2	0.5560249740	0.5779173382	0.5809582911	0.5820105072	0.5825676430	0.5829384293	0.5859005636
2	PRESENT 1	0.2224751220	0.2311430399	0.2323423490	0.2327559023	0.2329742650	0.2331193321	0.2342773810
	PRESENT 2	0.2224692776	0.2311414085	0.2323352828	0.2327446399	0.2329600317	0.2331029438	0.2342496562
3	PRESENT 1	0.1112899462	0.1155510400	0.1161346330	0.1163338865	0.1164383257	0.1165074286	0.1170603078
	PRESENT 2	0.1112832817	0.1155497579	0.1161282383	0.1163234683	0.1164250492	0.1164920775	0.1170341231
4	PRESENT 1	0.0655076788	0.0679543930	0.0682845078	0.0683955472	0.0684530943	0.0684909305	0.0687947118
	PRESENT 2	0.0654998961	0.0679535874	0.0682790285	0.0683862793	0.0684411212	0.0684769927	0.0687706264
5	PRESENT 1	0.0428679443	0.0444176550	0.0446224813	0.0446899283	0.0447243063	0.0447466952	0.0449273962
	PRESENT 2	0.0428587735	0.0444174411	0.0446181382	0.0446820876	0.0447139503	0.0447345103	0.0449059165

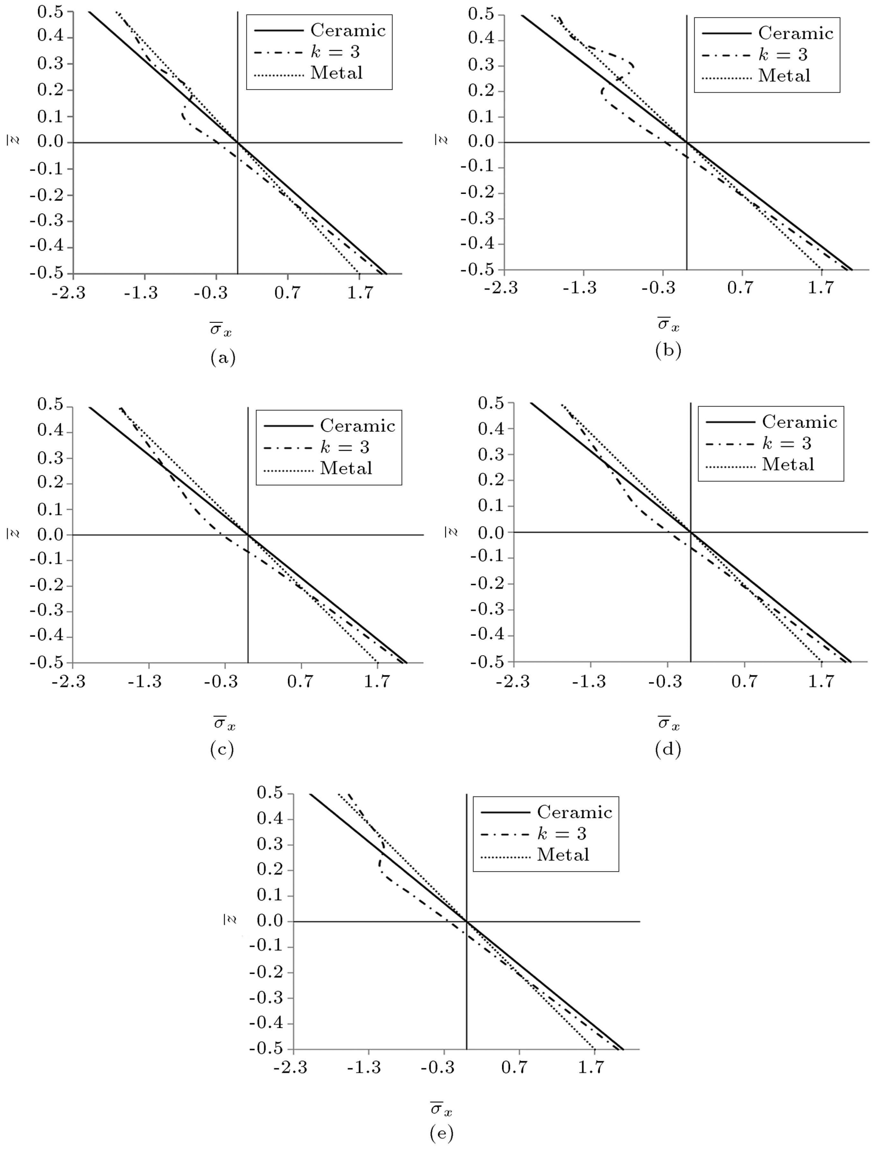

Figure 4. Distribution of dimensionless in-plane normal stress, $\overline{\sigma}_x$, through the dimensionless plate thickness for different thickness aspect ratios: (a) 1-1-1; (b) 1-2-1; (c) 1-2-2; (d) 2-1-2; and (e) 2-2-1.

Table 6. Effect of volume fraction index and thickness aspect ratio on in-plane normal stress, $\overline{\sigma}_x$ $(a/b = 1)$.

k	Theory	$\overline{\sigma}_x$				
		1-1-1	**1-2-1**	**1-2-2**	**2-1-2**	**2-2-1**
$k=0$	PRESENT 1	-1.666270185	-1.706173174	-1.750864976	-1.659805185	-1.659805183
	PRESENT 2	-1.666060872	-1.705227842	-1.749453161	-1.659980811	-1.659980815
	PSDPT	-1.666262293	-1.706145395	-1.750826730	-1.659809686	-1.659809686
	SSDPT	-1.666251551	-1.706108223	-1.750776194	-1.659815474	-1.659815474
	ESDPT	-1.666239223	-1.706067098	-1.750720991	-1.659821523	-1.659821523
	FSDPT	-1.666304291	-1.706320304	-1.751079099	-1.659775556	-1.659775556
$k=1$	PRESENT 1	-1.664537186	-1.650219824	-1.674486900	-1.670079883	-1.619779739
	PRESENT 2	-1.664869171	-1.650542326	-1.674474798	-1.670436590	-1.620452706
	PSDPT	-1.664547722	-1.650230005	-1.674485728	-1.670091315	-1.619803260
	SSDPT	-1.664561703	-1.650243499	-1.674484044	-1.670106492	-1.619834712
	ESDPT	-1.664577065	-1.650258299	-1.674481972	-1.670123219	-1.619869593
	FSDPT	-1.664478598	-1.650162909	-1.674488930	-1.670016939	-1.619654573
$k=2$	PRESENT 1	-1.665213426	-1.638296708	-1.670200987	-1.673283690	-1.591738489
	PRESENT 2	-1.665631213	-1.638845583	-1.670440685	-1.673668560	-1.592602883
	PSDPT	-1.665227609	-1.638315829	-1.670208133	-1.673296422	-1.591770112
	SSDPT	-1.665246589	-1.638341429	-1.670217557	-1.673313430	-1.591812491
	ESDPT	-1.665267691	-1.638369894	-1.670227809	-1.673332273	-1.591859600
	FSDPT	-1.665137762	-1.638195667	-1.670159390	-1.673214764	-1.591571828
$k=3$	PRESENT 1	-1.664947010	-1.630136403	-1.670966444	-1.674752458	-1.572213322
	PRESENT 2	-1.665395841	-1.630781411	-1.671289538	-1.675146085	-1.573191149
	PSDPT	-1.664962657	-1.630159716	-1.670976676	-1.674765667	-1.572249767
	SSDPT	-1.664983676	-1.630191030	-1.670990265	-1.674783330	-1.572298586
	ESDPT	-1.665007142	-1.630225994	-1.671005210	-1.674802960	-1.572352803
	FSDPT	-1.664864668	-1.630015106	-1.670909471	-1.674681466	-1.572021032
$k=4$	PRESENT 1	-1.664363446	-1.623612627	-1.672149528	-1.675553600	-1.557948963
	PRESENT 2	-1.664828430	-1.624314931	-1.672507898	-1.675950667	-1.559002872
	PSDPT	-1.664379907	-1.623638511	-1.672161178	-1.675567035	-1.557988595
	SSDPT	-1.664402048	-1.623673336	-1.672176696	-1.675585018	-1.558041661
	ESDPT	-1.664426828	-1.623712285	-1.672193837	-1.675605021	-1.558100490
	FSDPT	-1.664277475	-1.623478794	-1.672085743	-1.675481656	-1.557739052
$k=5$	PRESENT 1	-1.663711887	-1.618241874	-1.673152165	-1.676039216	-1.547094559
	PRESENT 2	-1.664187179	-1.618984220	-1.673527784	-1.676438015	-1.548203148
	PSDPT	-1.663728871	-1.618269574	-1.673164554	-1.676052770	-1.547136267
	SSDPT	-1.663751743	-1.618306856	-1.673181090	-1.676070932	-1.547192318
	ESDPT	-1.663777379	-1.618348574	-1.673199410	-1.676091156	-1.547254363
	FSDPT	-1.663623538	-1.618099111	-1.673084902	-1.675966745	-1.546871587

mum transverse shear stress is occurred at somewhere else than mid-plane. In all cases the shear stress, $\overline{\tau}_{xz}$, is zero at top and bottom of the plate and the free shear stress condition for plate surfaces is satisfied.

Example 2. A simply supported square FG sandwich plate subjected to a temperature field, varying linearly through the thickness and uniformly in x and y directions, is considered.

Since the obtained results for PRESENT 1 and PRESENT 2 formulations are very close and almost identical in Example 1, only results of former formulation will be presented. Convergence of solution for transverse deflection of plates with different volume fraction indexes is investigated in Table 8. As seen,

Table 7. Effect of volume fraction index and thickness aspect ratio on transverse shear stress, $\overline{\tau}_{xz}$ ($a/b = 1$, $\overline{T}_3 = -100$).

Scheme	Theory	$\overline{\tau}_{xy}$				
		1-1-1	**1-2-1**	**1-2-2**	**2-1-2**	**2-2-1**
$k = 0$	PRESENT 1	0.4028358771	0.4149608693	0.4240194720	0.4051912198	0.4051912198
	PRESENT 2	0.8185195399	0.8611282991	0.8977638131	0.8210835427	0.8210835454
	PSDPT	0.4835939258	0.5007396835	0.5128627023	0.4852054866	0.4852054866
	SSDPT	0.5934726419	0.6181984407	0.6348398250	0.5937493238	0.5937493238
	ESDPT	0.7175373248	0.7520809920	0.7112661898	0.7156444112	0.7156444068
$k = 1$	PRESENT 1	0.3432062880	0.3458099805	0.3766442324	0.3413718693	0.3130551319
	PRESENT 2	0.7049987498	0.7103409263	0.7730922364	0.7012350178	0.6447151154
	PSDPT	0.4122750313	0.4155986787	0.4527063288	0.4098902226	0.3762177188
	SSDPT	0.5065518345	0.5109037615	0.5564681898	0.5033668373	0.4625901791
	ESDPT	0.6131901777	0.6187806692	0.6739088205	0.6090165600	0.5603746910
$k = 2$	PRESENT 1	0.3088234924	0.3129745071	0.3491960938	0.3030138205	0.2875827468
	PRESENT 2	0.6391880299	0.6463100429	0.7164941693	0.6260836619	0.5935752116
	PSDPT	0.3715984124	0.3764347316	0.4194312529	0.3643737580	0.3458547636
	SSDPT	0.4575807395	0.4633035716	0.5152470741	0.4483249823	0.4256934533
	ESDPT	0.5552182657	0.5618162410	0.6235999229	0.5435454326	0.5162208151
$k = 3$	PRESENT 1	0.2910543906	0.2964798972	0.3287871582	0.2831556441	0.2824547146
	PRESENT 2	0.6049553154	0.6143239766	0.6763968230	0.5868641159	0.5821895481
	PSDPT	0.3506010343	0.3568666238	0.3950480248	0.3407837945	0.3396055396
	SSDPT	0.4323346531	0.4396710973	0.4855383249	0.4197559586	0.4179056687
	ESDPT	0.5253798864	0.5337292239	0.5879679250	0.5095093860	0.5066318196
$k = 4$	PRESENT 1	0.2825876839	0.2886603236	0.3130751787	0.2734689573	0.2819432394
	PRESENT 2	0.5888057166	0.5990913264	0.6457000803	0.5678457184	0.5798599671
	PSDPT	0.3406331613	0.3475981815	0.3763567704	0.3293006406	0.3388281774
	SSDPT	0.4204092018	0.4284919312	0.4628744336	0.4058869770	0.4167200219
	ESDPT	0.5113637840	0.5204565894	0.5609286709	0.4930374560	0.5048830244
$k = 5$	PRESENT 1	0.2789253711	0.2852696994	0.3010202953	0.2690055936	0.2821570433
	PRESENT 2	0.5820597330	0.5924169938	0.6221043826	0.5592639389	0.5790081723
	PSDPT	0.3363636015	0.3435750117	0.3620344454	0.3240416028	0.3389170908
	SSDPT	0.4153694582	0.4236361725	0.4455318450	0.3995865421	0.4165866368
	ESDPT	0.5055305868	0.5146810058	0.5402701760	0.4856232894	0.5043978689

Table 8. Convergence study of central transverse deflection, $\overline{w}$ (thickness aspect ratio: 1-2-1).

Volume fraction index	$\overline{w}$						
	$m = n = 1$	$m = n = 1..5$	$m = n = 1..10$	$m = n = 1..20$	$m = n = 1..30$	$m = n = 1..40$	$m = n = 1..50$
$k = 0$	0.9014	0.8144	0.8099	0.8084	0.8086	0.8085	0.8085
$k = 1$	0.9369	0.8465	0.8418	0.8403	0.8405	0.8404	0.8404
$k = 2$	0.9418	0.8510	0.8463	0.8447	0.8449	0.8449	0.8449
$k = 3$	0.9435	0.8525	0.8478	0.8462	0.8465	0.8464	0.8464
$k = 4$	0.9444	0.8534	0.8486	0.8471	0.8473	0.8472	0.8472
$k = 5$	0.9450	0.8539	0.8492	0.8476	0.8478	0.8478	0.8478

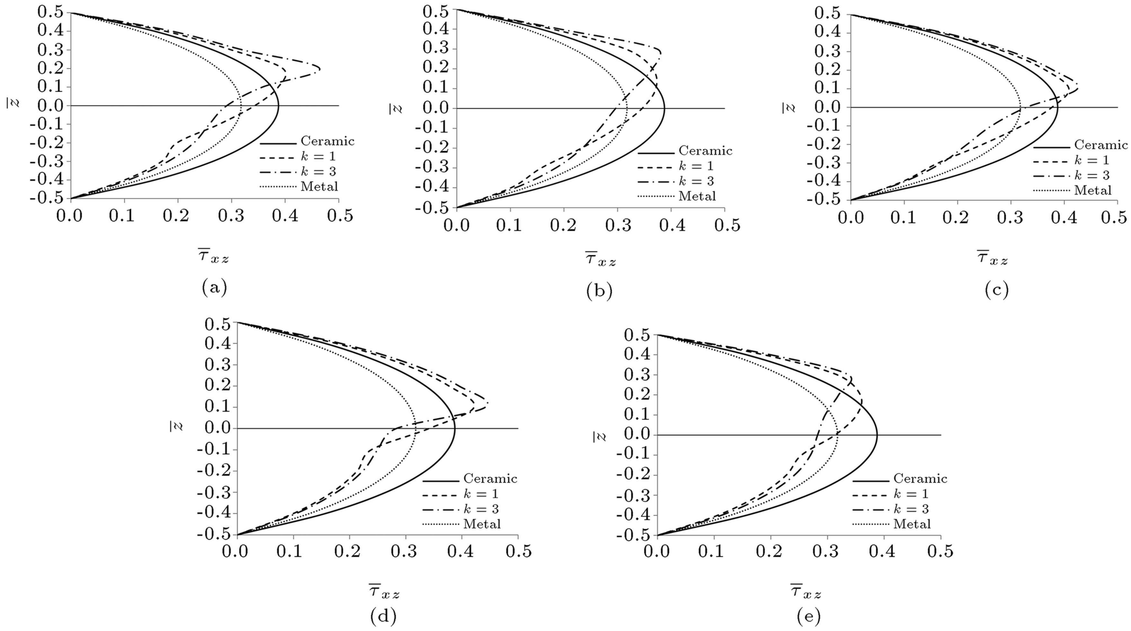

Figure 5. Distribution of dimensionless transverse shear stress, $\overline{\tau}_{xz}$, through the dimensionless plate thickness for different thickness aspect ratios: (a) 1-1-1; (b) 1-2-1; (c) 1-2-2; (d) 2-1-2; and (e) 2-2-1.

considering enough number of series terms, the obtained transverse deflections are quite converged. Table 9 presents the dimensionless transverse deflections considering different thickness aspect ratios and volume fraction indexes. It is observed that the transverse deflections are raised by increasing volume fraction index for all thickness aspect ratios. In comparison to sinusoidal temperature distribution, the obtained deflections have higher values.

Table 9. Effects of volume fraction index and thickness aspect ratio on dimensionless transverse deflection, $\overline{w}$.

Volume fraction index	$\overline{w}$				
	1-1-1	**1-2-1**	**1-2-2**	**2-1-2**	**2-2-1**
$k = 0$	0.8286	0.8085	0.7919	0.8380	0.8380
$k = 1$	0.8417	0.8404	0.8333	0.8428	0.8473
$k = 2$	0.8435	0.8449	0.8399	0.8435	0.8502
$k = 3$	0.8441	0.8464	0.8420	0.8737	0.8520
$k = 4$	0.8443	0.8472	0.8429	0.8438	0.8533
$k = 5$	0.8445	0.8478	0.8433	0.8440	0.8543

The convergence of solution for in-plane normal stresses, $\overline{\sigma}_x$, is investigated in Table 10. In comparison to transverse deflections, slow rate of convergences is observed for in-plane normal stress, $\overline{\sigma}_x$, because the stresses are computed from second derivatives of transverse deflections, and more terms in the related infinite series must be employed to achieve the desired accuracy.

Table 11 presents the dimensionless in-plane normal stress, $\overline{\sigma}_x$, for different thickness aspect ratios and volume fraction indexes. Like sinusoidal temperature field when volume fraction index is increased, the in-plane normal stress, $\overline{\sigma}_x$, is decreased for 1-2-1 and 2-2-1, increased for 2-1-2, and does not show regular changes for 1-1-1 and 1-2-2. In comparison to sinu-

Table 10. Convergence study of in-plane normal stress, $\overline{\sigma}_x$ (thickness aspect ratio: 1-2-1).

Volume fraction index	$\overline{\sigma}_x$							
	$m = n = 1$	$m = n = 1..50$	$m = n = 1..100$	$m = n = 1..200$	$m = n = 1..400$	$m = n = 1..600$	$m = n = 1..700$	$m = n = 1..800$
$k = 0$	-2.766	-1.747	-1.687	-1.697	-1.702	-1.703	-1.704	-1.704
$k = 1$	-2.676	-1.693	-1.628	-1.639	-1.645	-1.646	-1.647	-1.647
$k = 2$	-2.656	-1.682	-1.616	-1.627	-1.632	-1.634	-1.635	-1.635
$k = 3$	-2.643	-1.674	-1.607	-1.619	-1.624	-1.626	-1.627	-1.627
$k = 4$	-2.632	-1.667	-1.601	-1.612	-1.618	-1.620	-1.621	-1.621
$k = 5$	-2.623	-1.662	-1.595	-1.607	-1.612	-1.614	-1.615	-1.615

Table 11. Effects of volume fraction index and thickness aspect ratio on dimensionless in-plane normal stress, $\overline{\sigma}_x$.

Volume fraction index	$\overline{\sigma}_x$				
	1-1-1	**1-2-1**	**1-2-2**	**2-1-2**	**2-2-1**
$k=0$	-1.664	-1.704	-1.749	-1.657	-1.657
$k=1$	-1.662	-1.647	-1.672	-1.668	-1.617
$k=2$	-1.663	-1.635	-1.668	-1.671	-1.589
$k=3$	-1.662	-1.627	-1.668	-1.672	-1.569
$k=4$	-1.662	-1.621	-1.670	-1.673	-1.555
$k=5$	-1.661	-1.615	-1.671	-1.673	-1.544

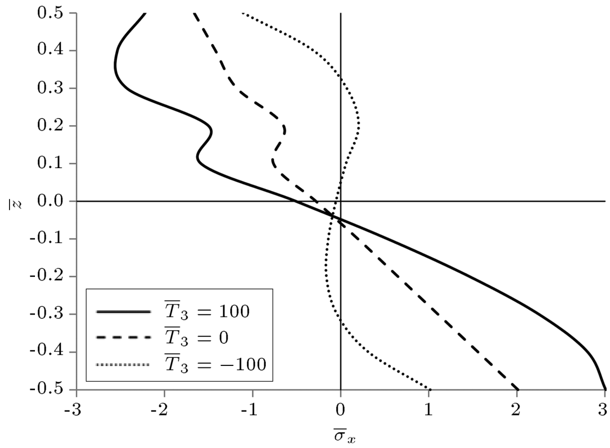

Figure 6. Effect of the thermal load value, $\overline{T}_3$, on distribution of dimensionless in-plane normal stress, $\overline{\sigma}_x$, through the dimensionless plate thickness (thickness aspect ratio: 1-1-1 and $k=3$).

soidal temperature field, the obtained in-plane normal stresses, $\overline{\sigma}_x$, are decreased for all thickness aspect ratios and volume fraction indexes.

Example 3. A simply supported square FG sandwich plate subjected to a temperature field distributed sinusoidally in x-y plane is considered. It is assumed that this field varies across the thickness according to Eq. (19) when $\overline{T}_1 = 0$, $\overline{T}_2 = 100$ and $\overline{T}_3$ takes different values. Figures 6 and 7 illustrate the effect of the thermal load value, $\overline{T}_3$, on dimensionless in-plane normal stress, $\overline{\sigma}_x$ and transverse shear stress, $\overline{\tau}_{xz}$. It is observed that thermal load value, $\overline{T}_3$, has a significant effect on in-plane normal and transverse shear stresses.

Example 4. A simply supported square FG sandwich plate subjected to a temperature field, distributed sinusoidally in x-y plane, is considered. It is assumed that this field varies across the thickness according to Eq. (19) when $\overline{T}_2 = 100$, $\overline{T}_3 = 0$, and $\overline{T}_1$ takes different values. Figures 8 and 9 illustrate the effect of the thermal load value, $\overline{T}_1$, on dimensionless in-plane

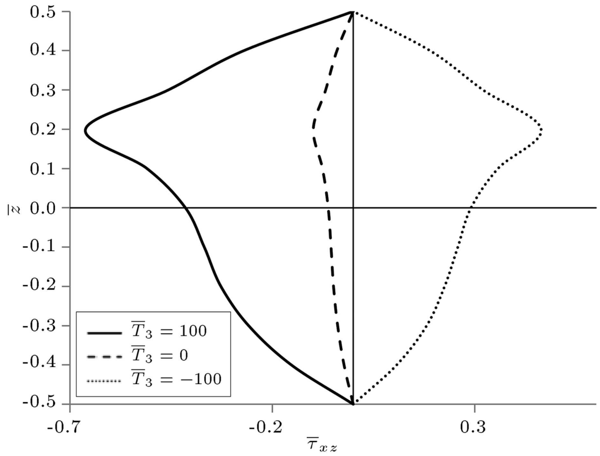

Figure 7. Effect of the thermal load value, $\overline{T}_3$, on distribution of dimensionless transverse shear stress, $\overline{\tau}_{xz}$, through the dimensionless plate thickness (thickness aspect ratio: 1-1-1 and $k=3$).

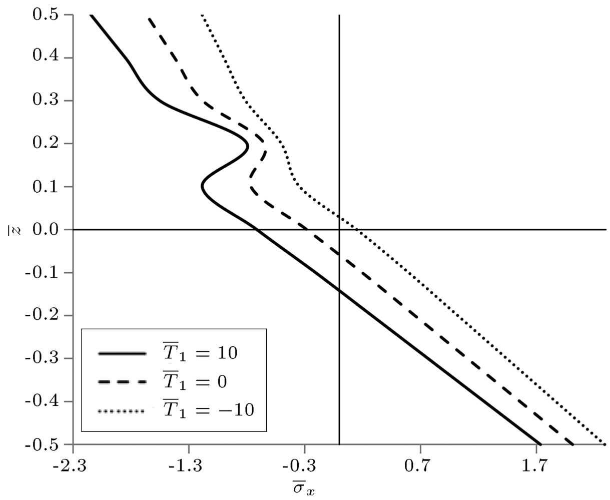

Figure 8. Effect of the thermal load value, $\overline{T}_1$, on distribution of dimensionless in-plane normal stress, $\overline{\sigma}_x$, through the dimensionless plate thickness (thickness aspect ratio: 1-1-1 and $k=3$).

normal stress, $\overline{\sigma}_x$, and transverse shear stress, $\overline{\tau}_{xz}$, and it is seen that these stresses are quite sensitive to $\overline{T}_1$.

5. Conclusions

In this paper, the hyperbolic shear deformation plate theory has been employed for thermo-elastic bending analysis of functionally graded sandwich plates. Governing equations were obtained with and without considering extension effect using the principle of virtual work; the Navier method was adopted for solution of the equations. Several thermo-mechanical benchmark problems were solved by presented formulation. Obtained results were compared with analytical solutions of other plate theories, and excellent agreement between present theory and other HSDTs

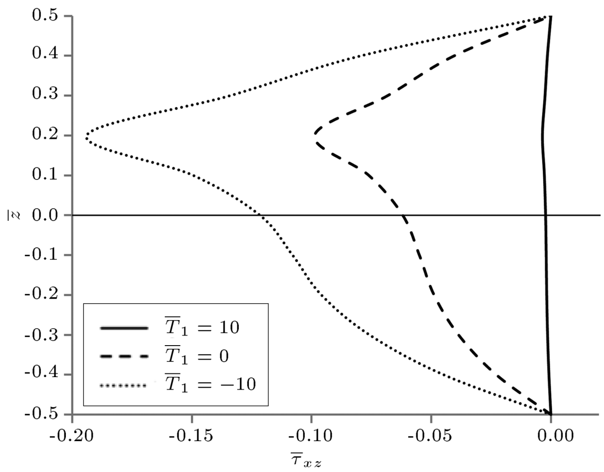

Figure 9. Effect of the thermal load value, $\overline{T}_1$, on distribution of dimensionless transverse shear stress, $\overline{\tau}_{xz}$, through the dimensionless plate thickness (thickness aspect ratio: 1-1-1 and $k = 3$).

was observed. It can be concluded that although simplicity is the main feature of presented formulation, it is completely accurate and efficient in thermo-elastic analysis of FG sandwich plates. The results indicated that elimination of extension term had no noticeable effect on the accuracy of the transverse deflections and in-plane normal stresses. However, the precision of the computed values for transverse shear stresses were quite affected by this term. Also the effect of thermal load, aspect ratio, thickness aspect ratio, thickness to side ratio and volume fraction index on obtained results were investigated and the results showed good consistency with expected trends.

References

1. Yamanouchi, M., Koizumi, M., Hirai, T. and Shiota, I. "FGM '90", *Proceedings of the First International Symposium on Functionally Gradient Materials*, Japan (1990).
2. Koizumi, M. "The concept of FGM", *Ceramic Transactions, Functionally Gradient Materials*, **34**, pp. 3-10 (1993).
3. Reddy, J.N. "Analysis of functionally graded plates", *Int. J. Numer. Method Eng.*, **47**(1-3), pp. 663-684 (2000).
4. Mechab, I., Mechab, B. and Benaissa, S. "Static and dynamic analysis of functionally graded plates using four variable refined plate theory by the new function", *Compos. Part B-ENG.*, **45**(1), pp. 748-757 (2013).
5. Zenkour, A.M. "Analytical solution for bending of cross-ply laminated plates under thermo-mechanical loading", *Compos. Struct.*, **65**(3-4), pp. 367-379 (2004).
6. Zenkour, A.M. and Alghamdi, N.A. "Thermoelastic bending analysis of functionally graded sandwich plates", *J. Mater. Sci.*, **43**, pp. 2574-2589 (2008).
7. Vaghefi, R., Baradaran, G.H. and Koohkan, H. "Three-dimensional static analysis of thick functionally graded plates by using meshless local Petrov-Galerkin (MLPG) method", *Eng. Anal. Bound. Elem.*, **34**(6), pp. 564-573 (2010).
8. Wu, C.P., Chiu K.H. and Wang, Y.M. "RMVT-based meshless collocation and element-free Galerkin methods for the quasi-3D analysis of multilayered composite and FGM plates", *Compos. Struct.*, **93**(2), pp. 923-943 (2011).
9. Wu, C.P. and Yang, S.W. "RMVT-based meshless collocation and element-free Galerkin methods for the quasi-3D analysis of multilayered composite and FGM circular hollow cylinders", *Compos. Part B-ENG.*, **42**(2), pp. 1683-1700 (2011).
10. Kashtalyan, M. "Three-dimensional elasticity solution for bending of functionally graded rectangular plates", *Eur. J. Mech. A/Solids*, **23**(5), pp. 853-864 (2004).
11. Vel, S.S. and Batra, R.C. "Three-dimensional exact solution for the vibration of functionally graded rectangular plates", *J. Sound Vib.*, **272**(3-5), pp. 703-730 (2004).
12. Reddy, J.N. "An evaluation of equivalent single layer and layerwise theories of composite laminates", *Compos. Struct.*, **25**(1-4), pp. 21-35 (1993).
13. Lanhe, W. "Thermal buckling of a simply supported moderately thick rectangular FGM plate", *Compos. Struct.*, **64**(2), pp. 211-218 (2004).
14. Zhao, X., Lee, Y.Y. and Liew, K.M. "Mechanical and thermal buckling analysis of functionally graded plates", *Compos. Struct.*, **90**(2), pp. 161-171 (2009).
15. Praveen, G.N. and Reddy, J.N. "Nonlinear transient thermo-elastic analysis of functionally graded ceramic-metal plates", *Int. J. Solids Struct.*, **35**(33), pp. 4457-4476 (1998).
16. Reddy, J.N. and Chin, C.D. "Thermo-mechanical analysis of functionally graded cylinders and plates", *J. Thermal Stress.*, **26**(1), pp. 593-626 (1998).
17. Kirchhoff, G. "Over the equilibrium and motion of an elastic disc" [Ä Uber das gleichgewicht und die bewegung einer elastischen scheibe], *J. Reine Angew. Math.*, **1859**(40), pp. 51-88 (1850).
18. Reissner, E. "The effect of transverse shear deformation on the bending of elastic plates", *J. Appl. Mech.*, **12**(2), pp. 69-77 (1945).
19. Mindlin, R.D. "Influence of rotary inertia and shear on flexural motions of isotropic elastic plates", *J. Appl. Mech.*, **18**(1), pp. 31-38 (1951).
20. Whitney J.M. and Sun, C.T. "A higher order theory for extensional motion of laminated composites", *J. Sound Vib.*, **30**(1), pp. 85-97 (1973).
21. Reddy, J.N. "A simple higher-order theory for laminated composite plates", *J. Appl. Mech.*, **51**(4), pp. 745-752 (1984).

22. Bhimaraddi, A. and Stevens, L.K. "A higher order theory for free vibration of orthotropic, homogeneous, and laminated rectangular plates", *J. Appl. Mech.*, **51**(1), pp. 195-198 (1984).

23. Lo, K.H., Christensen, R.M. and Wu, E.M. "A high-order theory of plate deformation, Part 1: Homogeneous plates", *J. Appl. Mech.*, **44**(4), pp. 663-668 (1977).

24. Shimpi, R.P. "Refined plate theory and its variants", *AIAA J.*, **40**(1), pp. 137-146 (2002).

25. Shimpi, R.P. and Patel, H.G. "A two variable refined plate theory for orthotropic plate analysis", *Int. J. Solids Struct.*, **43**(22-23), pp. 6783-6799 (2006).

26. Kim, S.E., Thai, H.T. and Lee, J. "A two variable refined plate theory for laminated composite plates", *Compos. Struct.*, **89**(2), pp. 197-205 (2009).

27. El Meiche, N., Tounsi, A., Ziane, N., Mechab, I. and Adda Bedia, E.A. "A new hyperbolic shear deformation theory for buckling and vibration of functionally graded sandwich plate", *Int. J. Mech. Sci.*, **53**(4), pp. 237-47 (2011).

28. Mantari, J.L and Guedes Soares, C. "A novel higher-order shear deformation theory with stretching effect for functionally graded plates", *Compos. Part B-ENG.*, **45**(1), pp. 268-281 (2013).

29. Tounsi, A., Houari, M.S.A., Benyoucef, S. and Adda Bedia, E.A. "A refined trigonometric shear deformation theory for thermoelastic bending of functionally graded sandwich plates", *Aerosp. Sci. Technol.*, **24**(1), pp. 209-220 (2013).

30. Mantari, J.L., Oktem, A.S. and Guedes Soares, C. "Bending and free vibration analysis of isotropic and multilayered plates and shells by using a new accurate higher-order shear deformation theory ", *Compos. Part B-ENG.*, **43**(8), pp. 3348-3360 (2012).

31. Vidal, P. and Polit, O. "A refined sinus plate finite element for laminated and sandwich structures under mechanical and thermomechanical loads", *Comput. Methods Appl. Mech. Engrg.*, **253**, pp. 396-412 (2013).

32. Zenkour, A.M. and Sobhy, M. "Dynamic bending response of thermoelastic functionally graded plates resting on elastic foundations", *Aerosp. Sci. Technol.*, **29**(1), pp. 7-17 (2013).

33. Houari, M.S.A., Tounsi, A. and Anwar Bég, O. "Thermoelastic bending analysis of functionally graded sandwich plates using a new higher order shear and normal deformation theory", *Int. J. Mech. Sci.*, **76**, pp. 102-111 (2013).

34. Wang, X. and Shi, G. "A simple and accurate sandwich plate theory accounting for transverse normal strain and interfacial stress continuity", *Compos. Struct.*, **107**, pp. 620-628 (2014).

35. Mantari, J.L. and Guedes Soares, C. "Optimized sinusoidal higher order shear deformation theory for the analysis of functionally graded plates and shells", *Compos. Part B-ENG.*, **56**, pp. 126-136 (2014).

36. Touratier, M. "An efficient standard plate theory", *Int. J. Eng. Sci.*, **29**(8), pp. 901-916 (1991).

37. Karama, M., Afaq, K.S. and Mistou, S. "Mechanical behavior of laminated composite beam by the new multi-layered laminated composite structures model with transverse shear stress continuity", *Int. J. Solids Struct.*, **40**(6), pp. 1525-1546 (2003).

38. Marur, P.R. "Fracture behavior of functionally graded materials", PhD Thesis, Auburn University, Alabama, (1999).

39. Chi, S.H. and Chung Y.L. "Mechanical behavior of functionally graded material plates under transverse load-Part II: Numerical results", *Int. J. Solids Struct.*, **43**(13), pp. 3675-3691 (2006).

40. Whitney, J.M. and Pagano, N.J. "Shear deformation in heterogeneous anisotropic plates", *J. Appl. Mech.*, **37**(4), pp. 1031-1036 (1970).

Biographies

Seyyed Jafar Rouzegar is currently an assistant professor at Faculty of Mechanical and Aerospace Engineering of Shiraz University of Technology, Iran. He received his BSc degree in Mechanical Engineering from Shiraz University, Iran, in 2002. He also received his MSc and PhD degrees in Mechanical Engineering from Tarbiat Modares University, Iran, in 2004 and 2010 respectively. His research interests include: FEM and XFEM, fracture mechanics and theories of plates and shells.

Mohammad Gholami is currently an MSc student at Faculty of Mechanical and Aerospace Engineering of Shiraz University of Technology, Iran. He received his BSc degree in Mechanical Engineering from Shahid Chamran University, Ahvaz, Iran, in 2011.